Out-of-Plane Polarization in Bent Graphene-Like Zinc Oxide and Nanogenerator Applications

Dan Tan, Morten Willatzen, and Zhong Lin Wang*

Highly efficient piezoelectric nanogenerator operation is demonstrated based on dynamic bending of graphene-like ZnO nanosheets. Energy is harvested by an external resistor by virtue of a strong time-varying piezoelectric polarization component perpendicular to the graphene-like ZnO plane. It is shown analytically and verified numerically using molecular dynamics simulations that the $\bar{6}$m2 point group of flat graphene-like ZnO is reduced to monoclinic m symmetry for bent graphene-like ZnO. The latter symmetry allows for a nonzero and large piezoelectric polarization component perpendicular to the plane of the 2D structure. The numerical results confirm that flexoelectric effects are negligible subject to graphene-like ZnO bending operation.

1. Introduction

Nanogenerators play an important and increasing role for energy harvesting and self-powered electronics.[1,2] 2D materials, such as transition metal dichalcogenides (e.g., MoS_2),[3,4] hexagonal boron-nitride (h-BN),[5,6] have been widely used in both piezoelectric[7,8] and triboelectric nanogenerators.[9,10] Typical for 2D materials are their combinations of high stiffness and an extremely low flexural rigidity.[11] Besides, lots of materials, even those that are nonpiezoelectric (centrosymmetric) in bulk systems, can become noncentrosymmetric and increasingly piezoelectric as the material thickness is reduced to a few monolayers or a single layer. Among all the piezoelectric 2D materials, group II oxides are short of study. In fact, materials of this group, like MgO, CaO, ZnO, CdO, have much higher piezoelectric coefficients compared to MoS_2 and

BN.[12] Wurtzite ZnO, shown in **Figure 1**a, is well known in piezoelectric nanogenerators.[13–16] By driving an atomic force microscope metal tip to slide over a ZnO nanowire array, or compressing a ZnO nanowire along the axial direction, one can get electrical power output. Recent studies (both theoretical[17,18] and experimental[19]) have shown that when the ZnO layer is thin enough, its wurtzite structure can transform into a 2D stable monolayer honeycomb structure similar to graphene and h-BN. Figure 1b shows the atomic structure of monolayer ZnO, where the geometrical parameters are $a = 3.21$ Å and $d = 1.85$ Å. This planar hexagonal structure is similar to graphene and named graphene-like ZnO.

To date, piezoelectricity research in 2D materials has mainly focused on the in-plane polarization.[20–23] Wu et al. proposed a single-layer MoS_2 piezoelectric device as shown in Figure 1c.[23] When the MoS_2 is bent, in-plane piezoelectric polarization is induced, which will generate opposite charges at the two ends. However, due to a high material stiffness, the mechanical strain that can be applied in a thermodynamically reversible manner is rather low, hence the attainable in-plane polarization is limited. On the contrary, the local polarization is linearly dependent on the curvature and can be large due to the material's low flexural rigidity.[24] In effect, a high output polarization and current can be generated by bending graphene-like ZnO in a dynamic fashion. The device can be designed like Figure 1d shows, where four distinct electrodes are placed on the layer's upper and lower sides. Bending of the 2D ZnO layer can generate piezoelectric outputs in both two external circuits with alternating polarity.

In the present analysis, a model of a bent graphene-like ZnO layer is built to study its out-of-plane polarization and its application in nanogenerators. The details are as follows: in Section 2, a symmetry analysis is conducted to understand the point group and symmetry characteristics of a bent ZnO nanosheet and the corresponding piezoelectric tensor. All the details of our molecular dynamics (MD) simulations are given in Section 3. In Section 4, simulation results show the relationships between radius of curvature, strain, and out-of-plane polarization. The piezoelectric coefficient e_{35} of the bent graphene-like ZnO is obtained afterward. Section 5 discusses effective application of a bent graphene-like ZnO layer in nanogenerators. Finally, conclusions of this paper are summarized in Section 6.

Dr. D. Tan, Prof. M. Willatzen, Prof. Z. L. Wang
CAS Center for Excellence in Nanoscience
Beijing Key Laboratory of Micro-Nano Energy and Sensor
Beijing Institute of Nanoenergy and Nanosystems
Chinese Academy of Sciences
Beijing 100083, China
E-mail: mortenwillatzen@binn.cas.cn
Dr. D. Tan, Prof. M. Willatzen, Prof. Z. L. Wang
School of Nanoscience and Technology
University of Chinese Academy of Sciences
Beijing 100049, China
Prof. Z. L. Wang
School of Materials Science and Engineering
Georgia Institute of Technology
Atlanta, GA 30332, USA

The ORCID identification number(s) for the author(s) of this article can be found under https://doi.org/10.1002/adfm.201907885.

ADVANCED
SCIENCE NEWS

www.advancedsciencenews.com
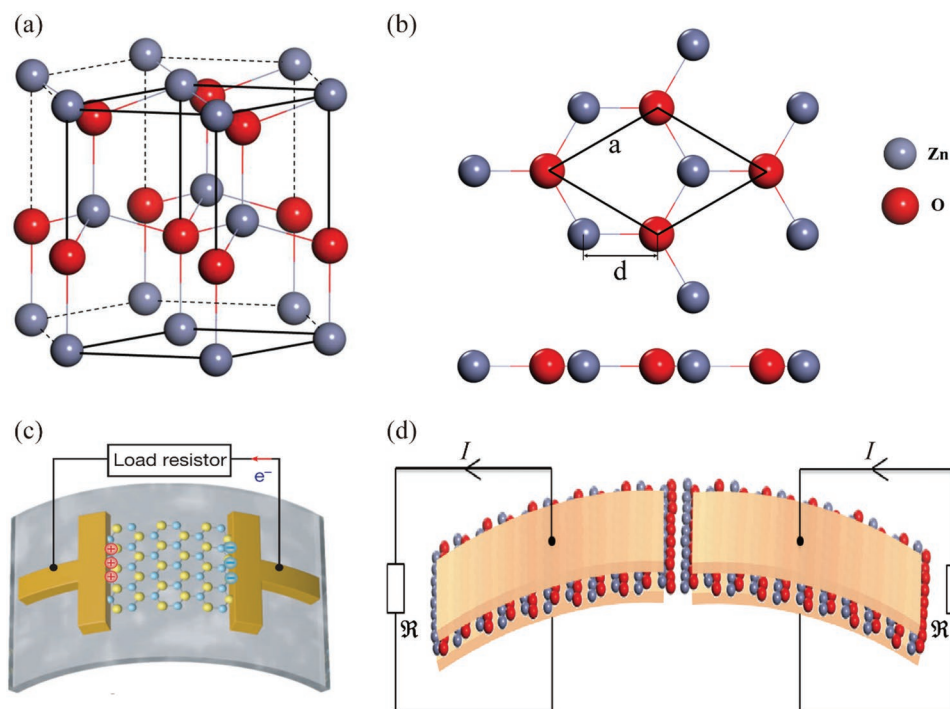
ADVANCED
FUNCTIONAL
MATERIALS

www.afm-journal.de

Figure 1. a) Schematic representation of a wurtzite ZnO structure. b) Top and side views of monolayer graphene-like ZnO. c) Operation scheme of the single-layer MoS$_2$ piezoelectric device.[23] d) Nanogenerator diagram of a bent graphene-like ZnO nanosheet.

2. Symmetry Analysis

Since flat monolayer graphene-like ZnO belongs to the $\bar{6}$m2 point group, only one free d- or one free e-coefficient exists. For piezoelectric e-coefficients the following relations apply

$$
\begin{aligned}
e_{111} &= e_{11} \\
e_{122} &= e_{12} = -e_{11} \\
e_{212} &= e_{221} = e_{26} = -e_{11}
\end{aligned}
\tag{1}
$$

So, the piezoelectric e tensor has the matrix form using Voigt notation

$$
e_{3\times6} = \begin{bmatrix}
e_{11} & -e_{11} & 0 & 0 & 0 & 0 \\
0 & 0 & 0 & 0 & 0 & -e_{11} \\
0 & 0 & 0 & 0 & 0 & 0
\end{bmatrix}
\tag{2}
$$

Using DFT-based Berry's phase approximation, we calculate the coefficient e_{11} to be 298 pC m^{-1}, which is consistent with other DFT results.[12,25]

Once a monolayer graphene-like ZnO is bent, even by a small external force, its $\bar{6}$m2 its symmetry is spontaneously broken.[26] We argue that the symmetry of the bent monolayer graphene-like ZnO belongs to the monoclinic m point group. **Figure 2** shows that two spatial operations are needed to form a symmetry operation. One is a rotation of 180° about the z-axis, the other a mirror operation in the y–z plane. The two operations are denoted 2 and m, respectively. Since this is the only spatial symmetry besides the trivial one (the identity operator) the structure belongs to the monoclinic m point group.

For the monoclinic m class, the piezoelectric stress matrix is

$$
e_{3\times6} = \begin{bmatrix}
e_{11} & e_{12} & e_{13} & 0 & e_{15} & 0 \\
0 & 0 & 0 & e_{24} & 0 & e_{26} \\
e_{31} & e_{32} & e_{33} & 0 & e_{35} & 0
\end{bmatrix}
\tag{3}
$$

It must be pointed out that bending will also generate strain gradients possibly leading to flexoelectricity. Therefore, the local polarization can have contributions from both piezoelectricity

Figure 2. Symmetry operation of bent graphene-like ZnO.

and flexoelectricity. We shall discuss the details in the following sections.

3. Molecular Dynamics Simulations

The simulated system, a bent 2D ZnO, is shown in **Figure 3**. Its dimensions are 96 Å along the x-axis and 104 Å along the y-axis. The total number of atoms in this system is 2196, i.e., 1098 Zn atoms and 1098 O atoms. The ZnO nanosheet is bent along the z-direction while both the left and right sides are fixed. The displacement vector therefore only has a z component.

All MD simulations are performed using the LAMMPS computational package.[27] The atomic interactions in the monolayer ZnO are described by a Buckingham-type potential.[28] The Buckingham potential has the form of $E = Ae^{-\frac{r}{\rho}} - \frac{C}{r^6}$, where A, ρ, and C are constants listed in **Table 1**, and r is the pair-wise distance. The long-range Coulomb electrostatic interactions are calculated by the damped shifted force model, which is a computationally efficient alternative to the Ewald summation.[29] All the MD simulations are carried out at room temperature ($T = 300$ K) within the NVT ensemble. To mimic realistic bending, we use a cylinder region as a bounding wall which interacts with ZnO particles according to Lennard-Jones 12/6 interactions. The axis of this cylinder region is in the y-direction, extending all the way to the global simulation box boundary. The x coordinate of cylinder's center coincides with the center of the monolayer ZnO, which is 0 in our cases. For the z direction, the cylinder moves along z axis over time with a speed of 0.005 A ps^{-1} to bend the dynamic parts of ZnO, while its two ends are kept fixed during the process of bending. Different cylinders induce different curvatures in the 2D structure.

4. Simulation Results

To better understand the bending process, we define the radius of curvature as R, then the bending curvature is derived as $1/R$. **Figure 4** shows the fitting curve of one bending configuration when the radius of curvature is 86 Å. The strain and strain gradient curves are obtained from the displacement fitting equation.

The fitting equation of the bending displacement can be written as
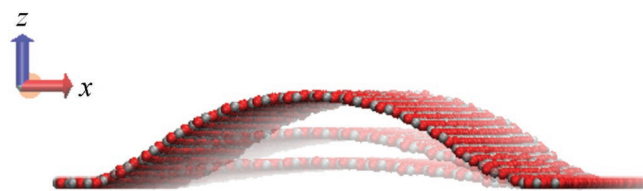
$$u_z(x) = -ax^2 + b \tag{4}$$

Figure 3. Bending configuration of a monolayer graphene-like ZnO membrane.

Table 1. Buckingham parameters for the Zn–O interactions.

Species	A [eV]	ρ [Å]	C [eV Å^6]
Zn^{2+}–Zn^{2+}	0.0	0.0	0.0
Zn^{2+}–O^{2-}	529.70	0.3581	0.0
O^{2-}–O^{2-}	9547.96	0.21916	32.0

where a and b are fitting parameters obtained directly from the MD simulations. Besides, a and b can be calculated mathematically from the following formulas

$$\frac{1}{R} = \left| \frac{\partial^2 u_z(x)}{\partial x^2} \right| = 2a \tag{5}$$

$$u_z(x_{max}) = -ax_{max}^2 + b = 0$$

Then we get $a = \frac{1}{2R}$ and $b = \frac{1}{2R}x_{max}^2$, where x_{max} is half of the length L_x of ZnO along the x direction.

Thus, the only strain component we have is s_{xz}

$$s_{xz} = \frac{1}{2}\frac{\partial u_z(x)}{\partial x} = -\frac{1}{2R}x \tag{6}$$

Note that since displacements are along the z-axis, $u_x(x) = 0$, and therefore $s_{xx} = 0$. As the strain is related to both $\frac{1}{R}$ and x, a larger strain is obtained by enlarging the curvature $\frac{1}{R}$ and/or the length of the 2D material along the x-axis.

Strain gradients are related to the flexoelectric polarization contribution. In our case, the only nonvanishing strain gradient component is always a constant

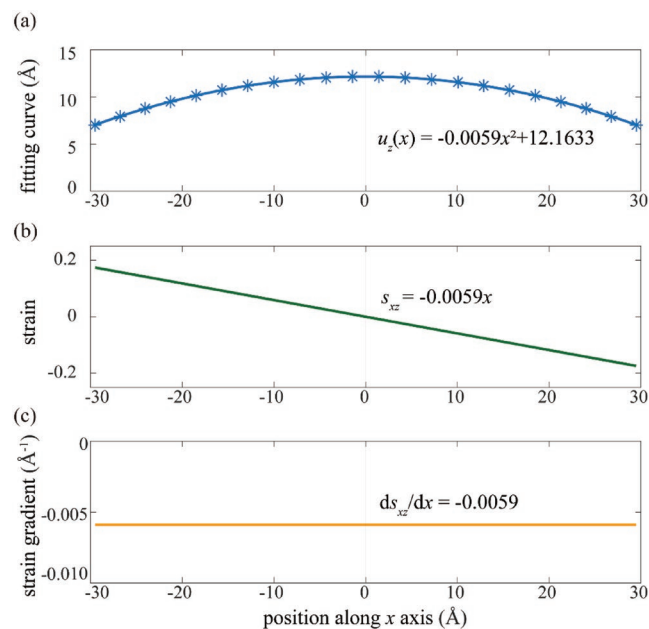$$\frac{\partial s_{xz}}{\partial x} = -\frac{1}{2R} \tag{7}$$

Figure 4. Fitting curve of the bending configuration when the curvature radius is 86 Å and its strain and strain-gradient curve.

The 2D polarization tensor is calculated as

$$P = \sum_i^N \frac{q_i r_i}{A} \qquad (8)$$

where q_i is the charge of the ith atom, r_i is the x-coordinate of the ith atom, N is the number of atoms, and A is the area of the flat membrane. The summation runs over all N atoms. From modern theory of polarization, one should work with changes in polarization rather than with absolute values.[4] In our case, the changes in polarization are the differences between the local polarization for any bending configurations and the initial local polarization where the latter corresponds to the flat 2D ZnO structure (i.e., the zero-strain case). Since the out-of-plane polarization is nonuniform we cut the monolayer ZnO into several uniformly sized regions along the x-axis so as to calculate the polarization distribution. **Figure 5** shows the polarization tensors along the x and z directions for different curvatures. Our simulations verify that the polarization change along the y-axis is zero. This result is in agreement with the monoclinic m symmetry for which e_{25} must be zero.

In Figure 5, we see that the amplitude of polarization P_z (green arrow) is much larger than P_x (yellow arrow) independent of the curvature. For nanogenerator operation, where the working principle is Maxwell's displacement current, it is the polarization change in time that leads to current and power output.[30] For bent graphene-like ZnO, the important quantity is the polarization along the z direction which is much larger than the polarization along the x direction. Further, contributions to P_z from surface area elements on one half plane of

the 2D material add together, and this is the reason for the choice of four separate electrodes to harvest energy. To explain this more clearly, the changes of P_z at different positions for different curvature radii are plotted in **Figure 6**a. Here we can see that P_z is a linear odd function of the x coordinate for a given curvature.

As mentioned above, the change of P_z can be divided into contributions from piezoelectricity and flexoelectricity. Since s_{xz} is the only nonzero strain component, the expression using Voigt notation is

$$P_3 = e_{35}s_5 + \mu_{313}f_{13} \qquad (9)$$

where $P_3 = P_z$, $s_5 = 2s_{xz}$, and $f_{13} = 2\frac{\partial s_{xz}}{\partial x}$.

Figure 6a reveals that P_3 is approximately zero when the x coordinate is zero independent of the curvature. Since the strain gradient is constant as a function of x and nonzero, this implies that the flexoelectric contribution can be neglected. This conclusion that monolayer graphene-like ZnO has a low flexoelectricity constant is consistent with Zhuang's work.[31] Hence, the second term in Equation (9) can be neglected.

Next, we consider several bending configurations corresponding to curvature radii R in the range between 86 and 366 Å. **Table 2** shows the obtained polarization values along the z-axis.

Figure 6b shows the dependency of P_z on the curvature $1/R$. Asterisks represent MD results. Evidently, P_z is proportional to $1/R$ and the proportionality constant is $\alpha = 187.8$ pC m^{-1}. The piezoelectric coefficient e_{35} for bent graphene-like ZnO is calculated using the following equation
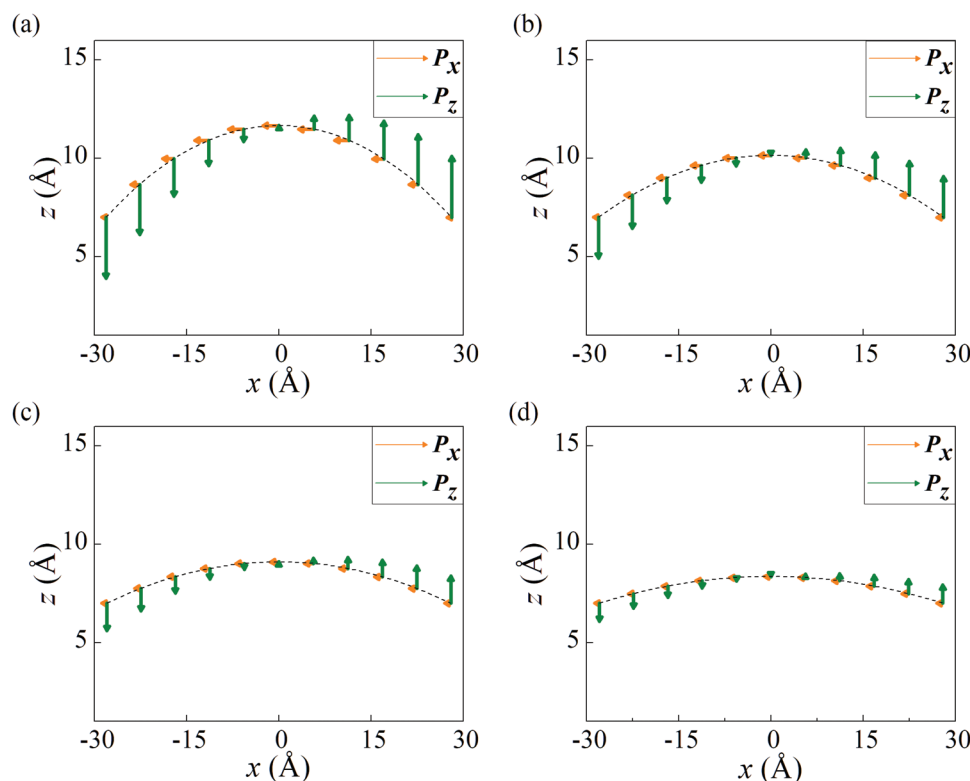

Figure 5. Polarization tensor of the bending monolayer ZnO membrane when the curvature radii are a) 86 Å, b) 126 Å, c) 186 Å, d) 286 Å, respectively.
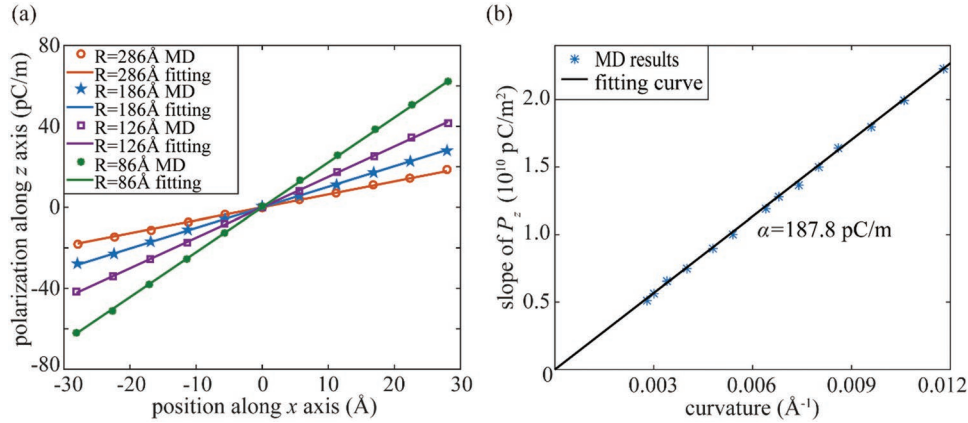
Figure 6. a) MD simulations of the polarization along the z-axis versus position along x-axis for different curvature radii. b) Fitting curve to calculate the piezoelectric constant e_{35} of bending graphene-like ZnO.

$$e_{35} = \frac{P_3(x)}{s_5(x)} = \frac{P_z(x)}{2s_{xz}(x)} = \frac{\frac{\alpha}{R}x}{-\frac{1}{R}x} = -\alpha = -187.8 \text{ pC m}^{-1} \tag{10}$$

5. Power Output of a Bent Graphene-Like ZnO Nanogenerator

In the previous sections the local polarization $P(x)$ at DC conditions was determined to be a function specified by the shear strain component $s_{xz}(x)$. Let us assume that at low vibrational frequencies, close to DC conditions, the local time-dependent polarization fulfills

$$P(x,t) = P(x)\exp(i\omega t) \tag{11}$$

where ω is the angular frequency of the vibration, equal to $2\pi f$. This assumption implies that all resonances of the 2D

Table 2. MD simulations of the polarization component along the z-axis for a variety of bending configurations.

Radius of curvature R [Å]	Strain $s_{xz} = -\frac{1}{2R}x$	Polarization along z-axis $P_z = \frac{\alpha}{R}x$ [pCm^{-1}]
366	$s_{xz} = -0.0014x$	$P_z = 0.512x$
326	$s_{xz} = -0.0015x$	$P_z = 0.561x$
286	$s_{xz} = -0.0017x$	$P_z = 0.657x$
246	$s_{xz} = -0.0020x$	$P_z = 0.747x$
206	$s_{xz} = -0.0024x$	$P_z = 0.899x$
186	$s_{xz} = -0.0027x$	$P_z = 1.003x$
156	$s_{xz} = -0.0032x$	$P_z = 1.190x$
146	$s_{xz} = -0.0034x$	$P_z = 1.281x$
136	$s_{xz} = -0.0037x$	$P_z = 1.364x$
126	$s_{xz} = -0.0040x$	$P_z = 1.498x$
116	$s_{xz} = -0.0043x$	$P_z = 1.639x$
106	$s_{xz} = -0.0048x$	$P_z = 1.798x$
96	$s_{xz} = -0.0053x$	$P_z = 1.994x$
86	$s_{xz} = -0.0059x$	$P_z = 2.227x$

graphene-like ZnO layer are sufficiently far away from the range of (small) frequencies relevant for typical nanogenerator operation.

Since we aim at a simple model for nanogenerator operation, we consider the following constitutive relation of 2D ZnO treated effectively as a 1D oscillator

$$\tilde{D} = \epsilon \tilde{E} + \tilde{P} \tag{12}$$

where the tilde denotes averaging over the half 2D ZnO plane, $\tilde{D}$ ($\tilde{E}$) is the averaged electric displacement (electric) field, ε is the permittivity of 2D ZnO, which is measured as 8.91.[32] These average values are defined as

$$\tilde{X} = \frac{1}{A}\int X(x)\,\mathrm{d}A \tag{13}$$

where $\tilde{X} = \tilde{D}, \tilde{E}, \tilde{P}$, $A = x_{max}L_y$, here L_y is the 2D layer length along the y direction.

We can now compute the generated output along the z direction assuming electrodes are deposited on both sides of the single layer of graphene as shown in **Figure 7**. Electric contact is broken along the edge $x = 0$, so we have two electrodes on the upper side of the 2D layer and two electrodes on the lower side. We denote the electrode on the upper left (upper right) side UL and the electrode on the lower left (lower right) side LL.

Recasting Equation (12) as

$$\tilde{E} = \frac{1}{\epsilon}\tilde{D} - \frac{1}{\epsilon}\tilde{P} \tag{14}$$

we obtain for the voltage across the 2D plane

$$V = -\int_{z_L}^{z_U} \tilde{E}_z\,dz = -\frac{\tilde{D}_z h}{\epsilon} + \frac{\tilde{P}_z h}{\epsilon}$$
$$= (\Re_i + \Re)A\frac{\partial \tilde{D}_z}{\partial t} = i(\Re_i + \Re)A\omega\tilde{D}_z \tag{15}$$

where z_U (z_L) are the upper (lower) z positions of the 2D ZnO material, h is the layer thickness, which is measured to 2.6 Å,[33] $\tilde{P}_z$ is the z component of the piezoelectrically generated average
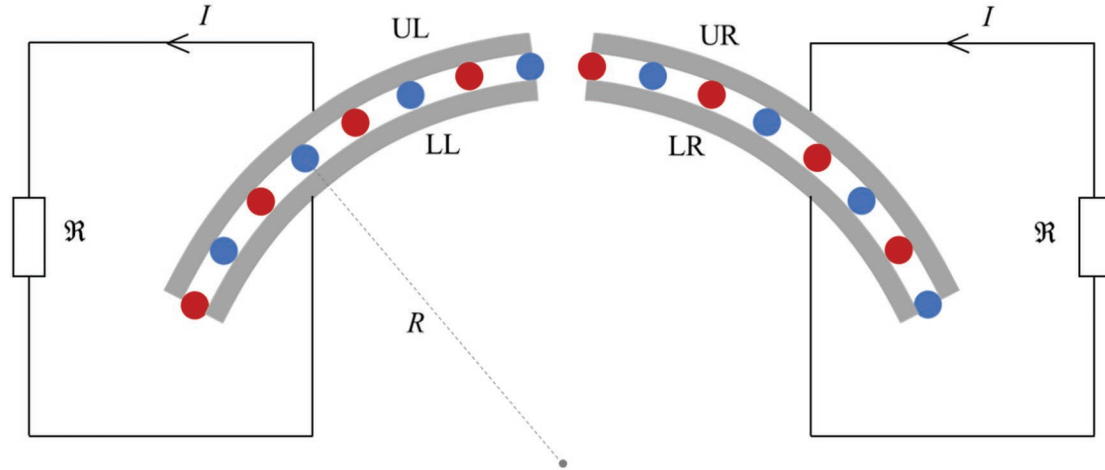
Figure 7. Schematic of a bent graphene-like ZnO nanogenerator.

polarization over the 2D plane, $\Re_i$ is the internal resistance of the half ZnO layer, $\Re$ is the load resistor, and we have used Kirchhoff's law to obtain the second-last equality. Further, it is assumed that the vibrational amplitude is small enough that the normal vector to the 2D ZnO plane points along the z direction at any time.

The internal resistance $\Re_i$ is given by

$$\Re_i = \frac{h}{\sigma A} \tag{16}$$

where σ is the conductivity of 2D ZnO, which is measured to ≈ 500 S m^{-1}.[34] Note that the combination of an atomic small thickness h of the 2D layer and the large area A of the half 2D ZnO plane guarantees that the internal resistance is very small, and can be made smaller by increasing the area of the 2D plane.

The averaged out-of-plane polarization $\tilde{P}_z$ can be derived from the above molecular dynamics simulation results. It should be noted that here the $P_z(x)$ is for bulk material, so we need to renormalize the above obtained polarization by the layer thickness h. Then the out-of-plane polarization can be rewritten as

$$P_z(x,t) = \frac{\alpha}{hR} x \exp(i\omega t) = -\frac{e_{35}}{hR} x \exp(i\omega t) \tag{17}$$

Thus, we have

$$\tilde{P}_z = \frac{1}{A} \int P_z(x) \, dA = -\frac{e_{35}}{2hR} x_{\max} \exp(i\omega t) \tag{18}$$

Solving Equation (15) for $\tilde{D}_z$ yields

$$\tilde{D}_z = \frac{1}{i\omega(\Re_i + \Re)A + \frac{h}{\epsilon}} \frac{\tilde{P}_z h}{\epsilon} = \frac{1}{e^{i\theta}\sqrt{\omega^2(\Re_i + \Re)^2 A^2 + \frac{h^2}{\epsilon^2}}} \frac{\tilde{P}_z h}{\epsilon}$$

$$= -\frac{1}{e^{i\theta}\sqrt{\omega^2(\Re_i + \Re)^2 A^2 + \frac{h^2}{\epsilon^2}}} \frac{e_{35}}{2\epsilon R} x_{\max} \exp(i\omega t) \tag{19}$$

where $\theta = \arctan\frac{\omega(\Re_i + \Re)A}{h/\epsilon}$.

We are now in a position to determine an expression for the time-dependent power generated by the movement of the half 2D ZnO layer harvested across one load resistor

$$\Pi(t) = \mathrm{Re}\left(i\Re A\omega\tilde{D}_z\right)\mathrm{Re}\left(iA\omega\tilde{D}_z\right) = \Re\left[\mathrm{Re}\left(iA\omega\tilde{D}_z\right)\right]^2 \tag{20}$$

where $\mathrm{Re}(x)$ denotes the real part of x. Note that Π depends on time since $\tilde{D}_z$ varies as $\exp(i\omega t)$.

Substituting Equation (19) into $iA\omega\tilde{D}_z$, we can obtain that

$$iA\omega\tilde{D}_z = -\frac{A\omega}{\sqrt{\omega^2(\Re_i + \Re)^2 A^2 + \frac{h^2}{\epsilon^2}}} \frac{e_{35}}{2\epsilon R} x_{\max} \exp\left(i\left(\omega t - \theta + \frac{\pi}{2}\right)\right) \tag{21}$$

Thus, its real part is given by

$$\mathrm{Re}\left(iA\omega\tilde{D}_z\right) = -\frac{A\omega}{\sqrt{\omega^2(\Re_i + \Re)^2 A^2 + \frac{h^2}{\epsilon^2}}} \frac{e_{35}}{2\epsilon R} x_{\max} \cos\left(\omega t - \theta + \frac{\pi}{2}\right) \tag{22}$$

Then the time-dependent power $\Pi(t)$ can be rewritten as

$$\Pi(t) = \frac{\Re A^2 \omega^2}{\omega^2(\Re_i + \Re)^2 A^2 + \frac{h^2}{\epsilon^2}} \frac{e_{35}^2}{4\epsilon^2 R^2} x_{\max}^2 \cos^2\left(\omega t - \theta + \frac{\pi}{2}\right) \tag{23}$$

The time average of the power, $\overline{\Pi}$, is given by

$$\overline{\Pi} = \frac{1}{T}\int_0^T \Pi(t)\,dt = \frac{1}{2}\frac{\Re A^2 \omega^2}{\omega^2(\Re_i + \Re)^2 A^2 + \frac{h^2}{\epsilon^2}} \frac{e_{35}^2}{4\epsilon^2 R^2} x_{\max}^2 \tag{24}$$

where $T = \frac{2\pi}{\omega}$ is the vibrational period.

It should be noted that this averaged power output is the contribution from one half of the 2D ZnO layer. The total harvested power is, therefore

$$\overline{\Pi}_{tot} = 2\overline{\Pi} = \frac{\Re A^2 \omega^2}{\omega^2 (\Re_i + \Re)^2 A^2 + \frac{h^2}{\epsilon^2}} \frac{e_{35}^2}{4\epsilon^2 R^2} x_{max}^2$$

$$= \frac{\Re A^2 \omega^2 e_{35}^2 x_{max}^2}{4 R^2 \left[\omega^2 \epsilon^2 (\Re_i + \Re)^2 A^2 + h^2 \right]}$$

(25)

The above expression provides a simple way to optimize the power output of a nanogenerator of this type. For a monolayer ZnO layer with dimensions $x_{max} = 2.5\,\mu m$ and $L_y = 5\,\mu m$ at 2.5 Hz, the relation between power output $\overline{\Pi}_{tot}$ and load resistance $\Re$ is shown in **Figure 8**a. The power output increases first as the load resistance increases, then decreased with increasing load. The maximum power is achieved for a load resistance of 8.392 GΩ and reaches 2.11×10^{-11} W. Comparing with the experimental result in ref. [23], its measured maximum instantaneous power delivered to the load reached 5.533×10^{-14} W. The main difference is the direction of the polarization driving the power output. Where we use the out-of-plane polarization to generate power, it is the in-plane polarization in ref. [23] that generates power. Although the materials are different, their piezoelectric coefficients e_{11} are almost the same ($e_{11} = 298\,pCm^{-1}$ for flat monolayer ZnO and $306\,pCm^{-1}$ for MoS_2). The high power output obtained in the present work shows that the out-of-plane polarization of bent 2D membranes with electrodes mounted on the nanosheet plane is suitable for energy harvesting.

Our calculations also reveal how the power output depends on the vibration frequency f, the ZnO layer length L_y along the y direction, and the half length x_{max} along the x direction. With the optimum load resistance, the power output $\overline{\Pi}_{tot}$ increases as the vibration frequency increases, where the dimensions are $x_{max} = 2.5\,\mu m$ and $L_y = 5\,\mu m$, as shown in Figure 8b. We can also see that at large frequency ($f > 10$ Hz), the power output is nearly unchanged. Figure 8c shows the power output $\overline{\Pi}_{tot}$ as a function of L_y while fixing the half length along the x direction to $x_{max} = 2.5\,\mu m$, the load resistance to $\Re = 8.392$ GΩ, and the vibration frequency to $f = 2.5$ Hz. As L_y increases, the power output is nearly constant when L_y is larger than 20 μm. With the same load resistance $\Re = 8.392$ GΩ and length $L_y = 5\,\mu m$ at $f = 2.5$ Hz, x_{max} is varied between 1 and 5 μm to get the variation of the power output shown in Figure 8d, which is quadratically in the ZnO layer dimension along the x direction (x_{max}).

6. Conclusion

Molecular dynamics simulations of the piezoelectric coefficient of bent graphene-like ZnO were carried out. It was demonstrated that the $\overline{6}m2$ point group symmetry of flat graphene-like ZnO is reduced abruptly (spontaneous symmetry breaking) to the monoclinic symmetry m point group subject to bending. This reduction in symmetry leads to a nonzero and large polarization component perpendicular to the graphene-like ZnO
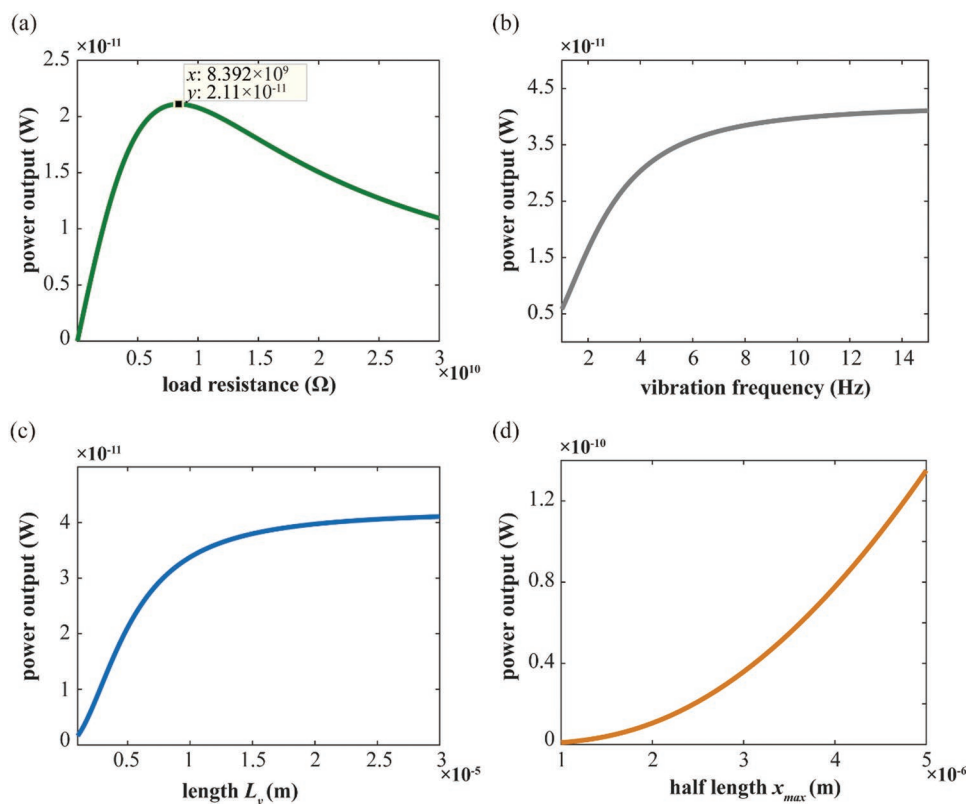

Figure 8. Dependency of total average power output $\overline{\Pi}_{tot}$ on a) load resistance $\Re$, b) vibration frequency f, c) length L_y along y direction, and d) half length x_{max} along x direction.

plane. We finally discussed highly efficient piezoelectric power output of bent graphene-like ZnO nanogenerators, by virtue of Maxwell's displacement current, as a result of the out-of-plane piezoelectrical polarization component. Our results also confirm that while piezoelectric effects are important, flexoelectric effects due to strain gradients are negligible in the case of bending of graphene-like ZnO.

Acknowledgements

Conflict of Interest

The authors declare no conflict of interest.

Keywords

[1] X. Pu, W. Hu, Z. L. Wang, *Small* **2018**, *14*, 1702817.
[2] F. R. Fan, W. Tang, Z. L. Wang, *Adv. Mater.* **2016**, *28*, 4283.
[3] Y. Zhou, W. Liu, X. Huang, A. Zhang, Y. Zhang, Z. L. Wang, *Nano Res.* **2016**, *9*, 800.
[4] D Tan, M. Willatzen, Z. L. Wang, *Nano Energy* **2019**, *56*, 512.
[5] M. López-Suárez, M. Pruneda, G. Abadal, R. Rurali, *Nanotechnology* **2014**, *25*, 175401.
[6] K. H. Michel, B. Verberck, *Phys. Rev. B* **2009**, *80*, 224301.
[7] R. Hinchet, U. Khan, C. Falconi, S.-W. Kim, *Mater. Today* **2018**, *21*, 611.
[8] S. A. Han, J. Lee, J. Lin, S. W. Kim, J. H. Kim, *Nano Energy* **2019**, *57*, 680.
[9] C. Wu, A. C. Wang, W. Ding, H. Guo, Z. L. Wang, *Adv. Energy Mater.* **2019**, *9*, 1802906.
[10] Z. Liu, H. Li, B. Shi, Y. Fan, Z. L. Wang, Z. Li, *Adv. Funct. Mater.* **2019**, *29*, 1808820.
[11] D. Akinwande, C. J. Brennan, J. S. Bunch, P. Egberts, J. R. Felts, H. Gao, R. Huang, J. S. Kim, T. Li, Y. Li, K. M. Liechti, N. Lu, H. S. Park, E. J. Reed, P. Wang, B. I. Yakobson, T. Zhang, Y. W. Zhang, Y. Zhou, Y. Zhu, *Extreme Mech. Lett.* **2017**, *13*, 42.
[12] M. N. Blonsky, H. L. Zhuang, A. K. Singh, R. G. Hennig, *ACS Nano* **2015**, *9*, 9885.
[13] Z. L. Wang, J. Song, *Science* **2006**, *312*, 242.
[14] Y. Gao, Z. L. Wang, *Nano Lett.* **2007**, *7*, 2499.
[15] S. Xu, Y. Qin, C. Xu, Y. Wei, R. Yang, Z. L. Wang, *Nat. Nanotechnol.* **2010**, *5*, 366.
[16] G. Romano, G. Mantini, A. Di Carlo, A. D'Amico, C. Falconi, Z. L. Wang, *Nanotechnology* **2011**, *22*, 465401.
[17] F. Claeyssens, C. L. Freeman, N. L. Allan, Y. Sun, M. N. R. Ashfold, J. H. Harding, *J. Mater. Chem.* **2005**, *15*, 139.
[18] Z. C. Tu, X. Hu, *Phys. Rev. B: Condens. Matter Mater. Phys.* **2006**, *74*, 035434.
[19] C. Tusche, H. L. Meyerheim, J. Kirschner, *Phys. Rev. Lett.* **2007**, *99*, 026102.
[20] K. N. Duerloo, M. T. Ong, E. J. Reed, *Environment* **2012**, *3*, 2871.
[21] S. K. Kim, R. Bhatia, T. H. Kim, D. Seol, J. H. Kim, H. Kim, W. Seung, Y. Kim, Y. H. Lee, S. W. Kim, *Nano Energy* **2016**, *22*, 483.
[22] J. Zhang, *Nano Energy* **2017**, *41*, 460.
[23] W. Wu, L. Wang, Y. Li, F. Zhang, L. Lin, S. Niu, D. Chenet, X. Zhang, Y. Hao, T. F. Heinz, J. Hone, Z. L. Wang, *Nature* **2014**, *514*, 470.
[24] T. Dumitrică, C. M. Landis, B. I. Yakobson, *Chem. Phys. Lett.* **2002**, *360*, 182.
[25] M. M. Alyörük, *Phys. Status Solidi B* **2016**, *253*, 2534.
[26] K. Brading, E. Castellani, *Symmetries in Physics: Philosophical Reflections*, Cambridge University Press, Cambridge **2003**.
[27] S. Plimpton, *J. Comput. Phys.* **1995**, *117*, 1.
[28] D. J. Binks, R. W. Grimes, *J. Am. Ceram. Soc.* **1993**, *76*, 2370.
[29] C. J. Fennell, J. D. Gezelter, *J. Chem. Phys.* **2006**, *124*, 234104.
[30] Z. L. Wang, *Mater. Today* **2017**, *20*, 74.
[31] X. Zhuang, B. He, B. Javvaji, H. S. Park, *Phys. Rev. B* **2019**, *99*, 054105.
[32] L. Wang, S. Liu, Z. Zhang, X. Feng, L. Zhu, H. Guo, W. Ding, L. Chen, Y. Qin, Z. Lin, *Nano Energy* **2019**, *60*, 724.
[33] H. T. Quang, A. Bachmatiuk, A. Dianat, F. Ortmann, J. Zhao, J. H. Warner, J. Eckert, G. Cunniberti, M. H. Rümmeli, *ACS Nano* **2015**, *9*, 11408.
[34] J. B. Baxter, C. A. Schmuttenmaer, *J. Phys. Chem. B* **2006**, *110*, 25229.